Ore Geology Reviews 53 (2013) 63–76

Contents lists available at SciVerse ScienceDirect

Ore Geology Reviews

journal homepage: www.elsevier.com/locate/oregeorev

Mineralogy, geochemistry and origin of Mn in the high-Mn iron ores, Bahariya Oasis, Egypt

Hassan M. Baioumy [a,*], Mohamed Z. Khedr [b], Ahmed H. Ahmed [c,1]

[a] Central Metallurgical R & D Institute, P.O. Box 87 Helwan, Cairo, Egypt
[b] Department of Geology, Faculty of Science, Kafr El Sheikh University, Egypt
[c] Department of Geology, Faculty of Science, Helwan University, Cairo, Egypt

ARTICLE INFO

Article history:
Received 24 February 2012
Received in revised form 29 November 2012
Accepted 10 December 2012
Available online 31 December 2012

Keywords:
Manganese
Iron ores
Bahariya Oasis
Egypt

ABSTRACT

Although Mn is one of the major impurities in the economic iron ores from the Bahariya Oasis, information on its modes of occurrence and origin is lacking in previous studies. High-Mn iron ores from El Gedida and Ghorabi–Nasser iron mines were subjected to detailed mineralogical, geochemical, and petrographic investigations using X-ray diffraction (XRD), infrared absorption spectrometry (IR), Raman spectroscopy, X-ray fluorescence (XRF), scanning electron microscopy (SEM), and electron probe microanalyzer (EPMA) to clarify the modes of occurrence of Mn in these deposits and its origin. The results showed that the MnO_2 contents range between 0.03 and 13.9 wt.%. Three mineralogical types have been identified for the Mn in the high-Mn iron ores, including: (1) inclusions within the hematite and goethite and/or Mn accumulated on their active surfaces, (2) coarse-grained and crystalline pyrolusite, and (3) fine-grained cement-like Mn oxide and hydroxide minerals (bixbyite, cryptomelane, aurorite, romanechite, manjiroite, and pyrochroite) between the Fe-bearing minerals. The Mn carbonate mineral (rhodochrosite) was detected only in the Ghorabi–Nasser high-Mn iron ores. Since IR patterns of low-Mn and high-Mn samples are almost the same, a combination of XRD analysis using non-filtered Fe-Kα radiations and Raman spectroscopy could be the best way to identify and distinguish between different Mn minerals.

Assuming that both Fe and Mn were derived from the same source, the occurrence of high-Mn iron ores at the base of the stratigraphic section of the deposits overlain by the low-Mn iron ores indicated a supergene origin of the studied ores by descending solutions. The predominance of Mn oxide and hydroxide minerals in botryoidal shapes supports this interpretation. The small grain size of Mn-bearing minerals as well as the features of microbial fossils such as spherical, elliptical, and filamentous shapes of the Fe-bearing minerals suggested a microbial origin of studied iron ores.

Variations in the distribution and mineralogy types of Mn in the iron ores of the Bahariya Oasis demanded detailed mineralogical and petrographic characterizations of the deposits before the beneficiation of high-Mn iron ores from the Bahariya Oasis as feedstock for the ironmaking industries in Egypt by magnetizing reduction. High Mn contents, especially in the Ghorabi–Nasser iron ore and occurrence of Mn as inclusions and/or accumulated on the surface of the Fe-bearing minerals would suggest a possible utilization of the high-Mn iron ores to produce ferromanganese alloys.

1. Introduction

Although manganese is added into steel for its deoxidizing and desulfurizing properties (e.g. Gutzmer and Beukes, 2002), the occurrence of Mn in the iron ore raw materials causes harm to the reduction process of iron oxides in the blast furnace. Mn forms strong oxides, which are partially reduced in the blast furnace with parts entering the slag. This is why the reduction behavior of Mn in the blast furnace was studied extensively before, trying to avoid the harmful effect of Mn in the ironmaking and steel industries (e.g. Atui et al., 1999; El Geassy et al., 2008; Terayama et al., 1996).

Due to the similarity of their chemical and physical properties, Fe and Mn are always associated in the Fe and Mn deposits throughout the geological record of different settings and origins. Urban et al. (1992) reported the formation of Mn and Fe ores in the Urucum District, Brazil via a supergene process. Corona-Esquivel et al. (2000) described Fe–Mn deposits in the Michoacan, Mexico that were formed as a result of hydrothermal precipitation. Saad et al. (1994) indicated that hydrothermal activity is mainly responsible for the formation of ferromanganese

* Corresponding author. Tel.: +20 225010642; fax: +20 225010639.
E-mail address: hassanbaioumy@hotmail.com (H.M. Baioumy).
[1] Current address: Faculty of Earth Sciences, King Abdulaziz University, Jeddah, Saudi Arabia.

0169-1368/$ – see front matter © 2012 Elsevier B.V. All rights reserved.
http://dx.doi.org/10.1016/j.oregeorev.2012.12.009

deposits from Um Bugma area, Egypt. According to Mohapatra et al. (2009), the in situ Fe and Mn deposits at Koira-Noamundi province, India represent exhalative phases of volcanism along the fracture zone where Mn was discharged along with Fe.

Several iron ore deposits are located in Bahariya Oasis, Egypt, e.g., El Harra, El Heiz, Ghorabi, El Gedida, and Nasser areas. The iron ore of El Harra belongs to El Harra member of El Haffuf Formation; whereas El Gedida iron ore belongs to the Naqb Formation (Basta and Amer, 1969; El Bassyony, 1970, 2000). The proven reserves of iron ores in the Bahariya Oasis is about 270 million metric tons and are produced from El Gedida mine as raw material for the Egyptian Steel Company (ESC). Nakhla and Shehata (1967) classified the iron ores from the Bahariya Oasis into four types; (i) pisolitic ores, (ii) hard goethitic ores, (iii) soft ores with relatively high Mn contents, and (iv) ochreous ore. Although Mn occurs in significantly high concentrations in some of these deposits and represents one of the major impurities in these deposits along with barite and halite, its mode of occurrence, relation with Fe-bearing minerals and source of metals are lacking in the previous research works. Identification and distinction between various Mn and Mn-bearing minerals was also problematic. In the current paper, representative samples from the iron ores of the Bahariya Oasis, especially high-Mn iron ores, were investigated for their petrography, mineralogy, and geochemistry to clarify the mode(s) of occurrence of Mn and its relation to Fe-bearing phases. The results were discussed to examine the possible source(s) of Mn in the deposits as well as the origin of iron ores in general.

2. Geology and stratigraphy of the iron ores

The Bahariya Oasis is a large depression in the Western Desert of Egypt with hot, arid climatic conditions. It is located about 270 km SW of Cairo and 180 km west of the Nile Valley (Fig. 1). Economic iron ore deposits with an average of 47.6 wt.% of Fe (Said, 1990) occur in the Bahariya Oasis. The ores are situated at the northern part of the depression and extend over an area of 11.7 km^2 with a thickness varying from 2 to 35 m, averaging 9 m (Said, 1990). The

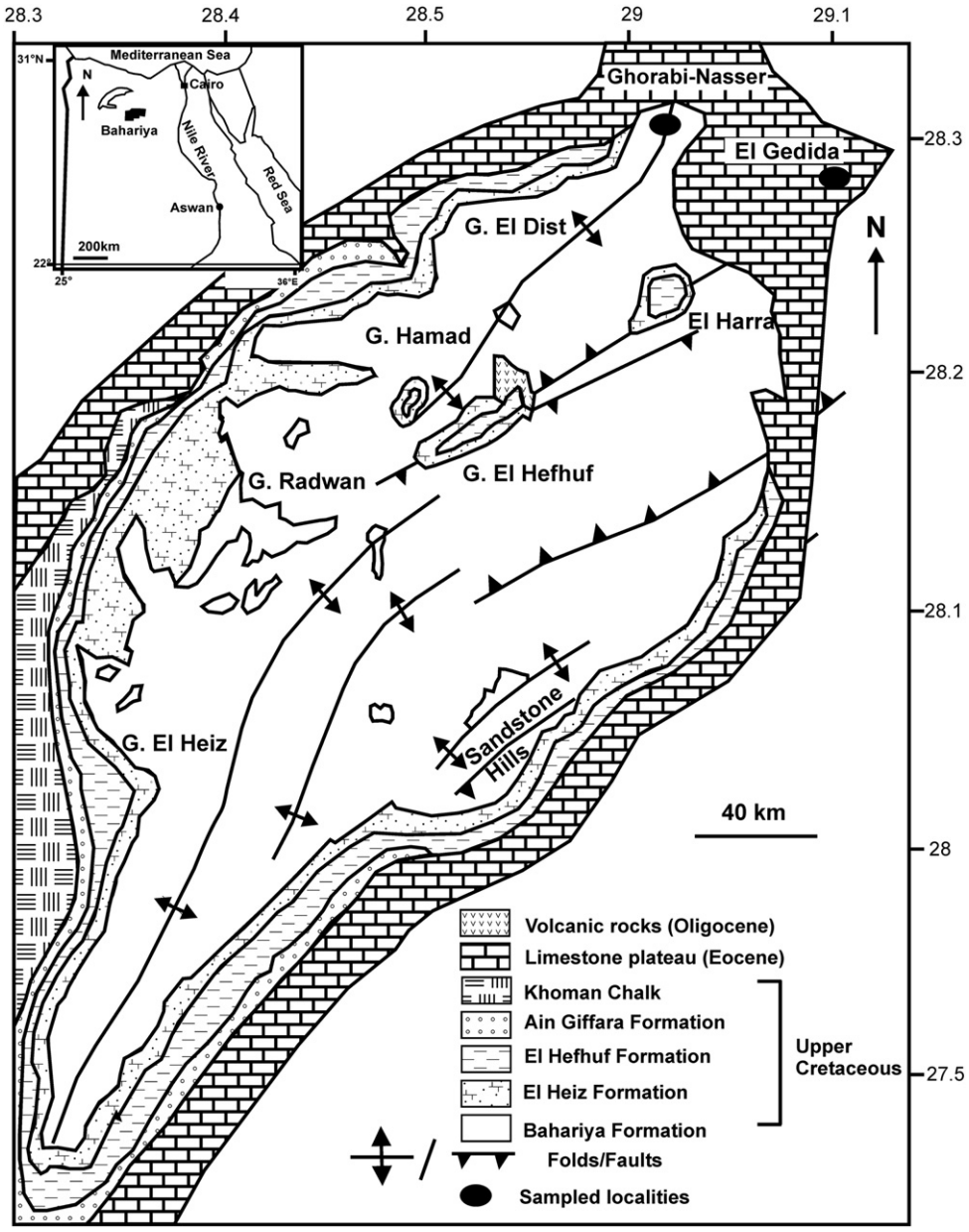

Fig. 1. Generalized geological map of the Bahariya Oasis, Western Desert, Egypt with the location of the studied Fe ores (after Catuneanu et al., 2006).

iron ores in the northern Bahariya Oasis are confined to the lower part of the Middle Eocene limestone of the Naqb Formation. The Naqb Formation ranges in thickness between 8 and 11.6 m and is composed of hard yellowish brown crystalline limestone with marl intercalations (El Bassyony, 2005). The iron ores occur in three areas: (i) Ghorabi–Nasser (3.5 km^2); (ii) El Harra (2.9 km^2); and (iii) El Gedida (15 km^2). Since the current study focuses on the iron ores in Ghorabi–Nasser and El Gedida due to their relatively large reserves of iron ores, detailed geology and stratigraphy of these two areas will be addressed in this section.

The El Gedida iron mine area is an oval shaped depression up to 15 km^2 in area, situated within the degraded cone hills of the Naqb Formation. The central part of the depression is characterized by a high relief (up to 254 m above sea level). The low Wadi area, up to 198 m above sea level, surrounds the high central area, which comprises the Cenomanian sandstone and sandy clays of the Bahariya Formation at the base, overstepped by the main Lutetian iron ore successions of the Naqb Qazzun Sequence. In the Eastern and Western Wadi areas, the ore successions are truncated unconformably by late Lutetian–Bartonian glauconitic sediments with lateritic ironstone interbeds of the Hamra Formation. The iron ore sequence attains its maximum thickness, up to 35 m, in the Eastern and Western Wadi areas, and it is much reduced in the high Central area where it attains a thickness of only 11 m. This iron ore sequence consists of a pisolitic–oolitic ironstone unit followed by bedded karst iron ores intercalated with ferruginous mudstones (Fig. 2A) (e.g. El Aref et al., 1999). The thickness of the overlying glauconitic sandstone of the Hamra Formation varies from ≤25 m in the Western and Eastern Wadis areas to <1 m in the high central area. High-Mn iron ores in the El Gedida mine occur as pockets of brownish gray friable materials (Fig. 2B) in the lower parts of the mined areas and are usually excluded from the iron ore production.

The exposed sedimentary sequence at Ghorabi–Nasser (Fig. 3A) starts at its base with sediments of the Bahariya Formation that are composed of moderately hard gray to yellowish gray clayey sediments that are overlain by glauconitic sandstone beds ranging in thickness from 20 cm to 1 m and are separated by iron-rich bands and concretions. The total thickness of glauconite-bearing unit is approximately 4 m and is overlain by the Naqb Qazzun Sequence starting with yellowish white soft to moderately hard, laminated clayey sediments of about 3 m thick and intercalated with iron-rich bands and concretions. Overlying these yellowish white sediments, the iron ores ranging in thickness from 6 to 10 m and occur as massive and brown ore with some reddish bands of ochre. Salama et al. (2012) subdivided this succession into lower and upper sequences. The lower sequence is a lagoonal manganiferous and fossiliferous ironstone facies association. The upper sequence is a peritidal microbially mediated stromatolitic and nummulitic–ooidal–oncoidal ironstone facies association. The iron ore beds are generally capped by an alluvial cover and/or quartzites of approximately 50 cm in thickness. In the Ghorabi–Nasser area, high-Mn iron ores are located in the lower most part of the sedimentary sequence as moderately hard, massive, brownish gray ores (Fig. 3B).

3. Materials and analytical methods

High-Mn iron ores from the Ghorabi–Nasser area (1 sample) and El Gedida iron mine (2 samples) in addition to high grade (low-Mn) iron ores (2 samples) and ochre (3 samples) from both areas were collected and subjected to detailed petrographic, mineralogical, and geochemical investigations. Polished sections were prepared and investigated using a conventional optical microscope. Sample powders were analyzed for their mineralogical composition using X-ray powder diffraction (XRD) technique using a Philips PW 1730 X-ray generator with Ni-filtered Cu-Kα, Fe-filtered Co-Kα, and non-filtered Fe-Kα runs at 40 kV and 25 mA to identify the Mn-bearing minerals as well as Fe-bearing phases. Morphology and chemistry of Fe- and Mn-bearing minerals were investigated by SEM-EDS Jeol-JSM 5410 at an operating voltage of 80 kV and a beam current of 20 μA. High-resolution imaging was conducted at magnifications between 3500× and 10,000×. Infrared vibrational spectrum (IR) of iron ore powdered samples in KBr is recorded on Fourier Transform and Pye-Unicam SP 300 instrument. Petrography, XRD, and IR analyses were performed at the Central Metallurgical R & D Institute (CMRDI), Cairo, Egypt. Elemental distribution mapping and mineral chemistry of selected samples were performed in thin polished sections using a JEOL electron-probe

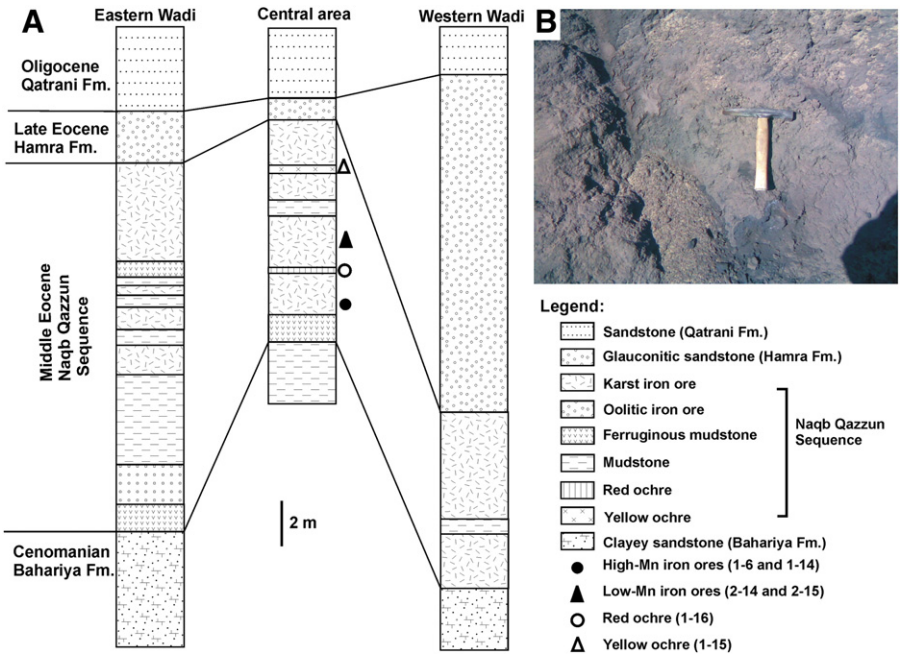

Fig. 2. (A) Stratigraphic section of the iron ores in the El Gedida iron mine (after El Aref et al., 1999). (B) Field photograph of the high-Mn iron ores in the El Gedida area. Hammer is approximately 20 cm in length.

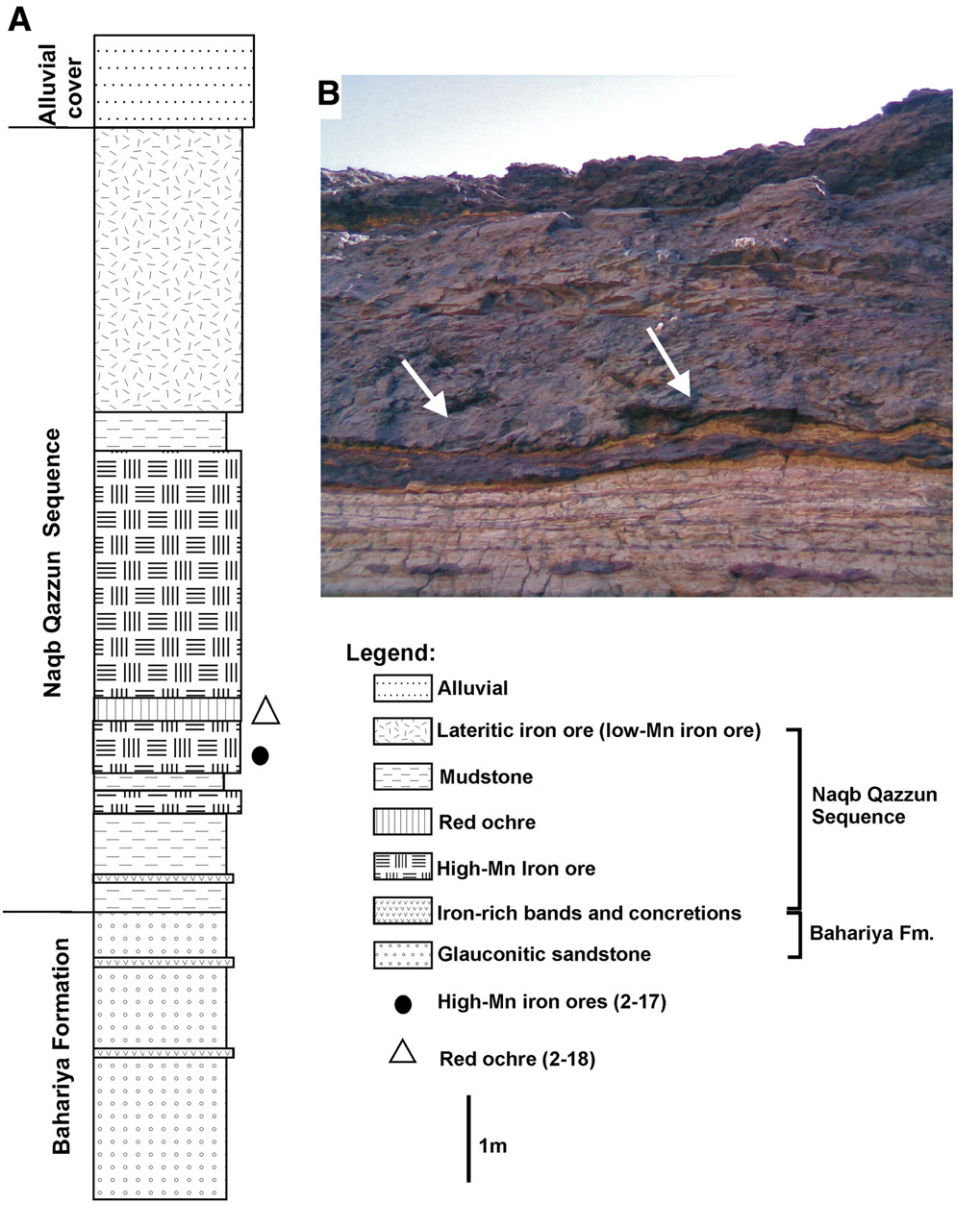

Fig. 3. (A) Stratigraphic section of the iron ores in the Ghorabi–Nasser area. (B) Field photograph of the high-Mn iron ores in the El Gedida area. Arrows refer to the sampled high-Mn horizon at the lower part of the section.

microanalyzer JXA-8800 at the Center for Cooperative Research of Kanazawa University, Japan. Analytical conditions were 20-kV accelerating voltage, 20-nA probe current, 3 μm probe diameter and the counting time was 10 s for each element. The raw data were corrected with an online ZAF program. Standards used for oxide and silicate minerals are natural minerals such as: quartz for silicon (Si), eskolite for chromium (Cr), fayalite for iron (Fe), wollastonite for calcium (Ca), corundum for aluminum (Al), periclase for magnesium (Mg), manganosite for manganese (Mn), jadeite for sodium (Na), orthoclase for potassium (K) and nickel oxide for nickel (Ni). Representative samples of the high Mn iron ores from El Gedida and Ghorabi–Nasser areas were broken into small pieces with fresh surfaces for Raman spectroscopic analyses. The Raman system (HORIBA Jobin Yvon, LabRAM HR800), at Kanazawa University, Japan was equipped with a 514.5 nm Ar laser (MELLES GRIOT, 43 SERIES ION LASER, 543-GS-A02) and an optical microscope to identify the Mn–Fe phases. The laser beam with a spatial resolution of about 1 μm and an irradiation power of 0.92 mW at the sample surface was focused through a 100-μm entrance pinhole and a 100× objective lens. This system was equipped with a charge-coupled device detector (1024×256 pixels). A pinhole diameter of 300 μm and a slit with 100 μm in width were positioned in front of the spectrometer. The Raman shift was below 70 cm^{-1}. The spectrometer was calibrated by using the Si 520 cm^{-1} peak with precisions lower than 0.5 cm^{-1}. By using a LabSpec (ver.5) software package, the Raman spectra with a spectral range of 0–2000 cm^{-1} for Mn–Fe phases was obtained. The 600-lines/mm grating for Mn–Fe phases was used to give a wavenumber resolution of 0.4—0.5 cm^{-1} and a spectral resolution of about ±0.8 to ±1.0 cm^{-1} in the spectral range.

Fused disks prepared from representative samples were analyzed for their major oxides by XRF using Philips PW 2400 X-ray fluorescence (XRF) spectrometer at Tohoku University, Japan. Tube voltage and current for W target were 40 kV and 60 mA, respectively. Loss on ignition (L.O.I.) was obtained by heating sample powders to 1000 °C for 6 h. Samples and the used methods of the Ghorabi–Nasser and El Gedida areas are summarized on Table 1.

Table 1
Summary of iron ore samples collected from El Gedida and Ghorabi–Nasser areas and types of analyses performed on these samples.

Area	Samples	Ore type	Analyses
El Gedida	2-14	Low-Mn iron ore	XRD, XRF, SEM, DTA, EPMA
	2-15	High-Mn iron ore	XRD, XRF, SEM, DTA, EPMA
	1-6	High-Mn iron ore	XRD, XRF
	1-14	High-Mn iron ore	XRD, XRF, SEM, DTA, EPMA
	1-15	Yellow ocher	XRD, XRF
	1-16	Red ocher	XRD, XRF
Ghorabi-Nasser	2-17	High-Mn iron ore	XRD, XRF, SEM, DTA, EPMA
	2-18	Red ocher	XRD, XRF

4. Results

4.1. Major oxides distribution

Data of XRF analyses of eight selected samples of El Gedida and Ghorabi–Nasser iron ores, Bahariya Oasis are shown in Table 2. MnO_2 contents vary between 0.03 and 13.9 wt.%. Some of the iron ores from El Gedida area, which are called high-Mn iron ores, show considerably high MnO_2 contents (7.5 to 8.8 wt.%). A sample from the lower part of the iron ores at the Ghorabi–Nasser area has the highest MnO_2 content (13.9 wt.%). Although yellow and red ochre samples from El Gedida mine have very low MnO_2 contents (0.03 and 0.12 wt.%, respectively), the red ochre sample from the Ghorabi–Nasser area has relatively high MnO_2 content (3.58 wt.%). In the high-Mn samples (7.5 to 13.9 wt.% MnO_2), MnO_2 shows strong negative correlation with the Fe_2O_3 contents ($r^2 = 0.8$, $n = 5$). Fe_2O_3 contents in the analyzed samples range between 40.1 and 88.6 wt.% with an average of 54.9 wt.%. SiO_2 and Al_2O_3 contents are generally low (averages of 0.9 and 1.2 wt.%, respectively) with an exceptional high SiO_2 and Al_2O_3 contents in the red ochre from the Ghorabi–Nasser iron ores (13.7 and 4.7 wt.%, respectively). The average contents of TiO_2, CaO, MgO, Na_2O, K_2O, and P_2O_5 are relatively low in all analyzed samples (averages of 0.4, 0.8, 0.6, 0.7, 0.1, and 0.2 wt.%, respectively).

4.2. Mineralogy

4.2.1. XRD

XRD analysis indicated the presence of several Mn-bearing minerals in the high-Mn iron ores from the Bahariya Oasis (Table 3). Pyrolusite (MnO_2) was identified in the XRD pattern by its characteristic peak at 3.12 Å in the Ni-filtered Cu-Kα, Fe-filtered Co-Kα, and non-filtered Fe-Kα runs in a sample from El Gedida area that contains 27 wt.% MnO_2. Samples with higher Mn contents (3.6 to 13.9 wt.% MnO_2) from El Gedida and Ghorabi–Nasser do not have pyrolusite in their mineralogical compositions. Mn-bearing minerals in these samples are dominated by a mixture of Mn oxides and hydroxide minerals. Mn oxide minerals are represented by bixbyite $(Mn,Fe)_2O_3$, cryptomelane $(Mn,K)_8O_6$, aurorite (Mn,Ca, $Ag)_3O_7 \cdot 3(H_2O)$, romanechite $(Ba,H_2O)_2(Mn)_5O_{10}$, and manjiroite $(Na,K)(Mn)_8O_{16} \cdot n(H_2O)$. Mn hydroxide minerals occur as pyrochroite $(Mn(OH)_2$, according to determination by different filtered conditions. Mn carbonate minerals occur as rhodochrosite ($MnCO_3$) only in the Ghorabi–Nasser high-Mn iron ores. Aurorite is the only mineral in this association that was identified in the Fe-filtered Co-Kα run. Other minerals appeared only in the non-filtered Fe-Kα run. In all samples, the Fe-bearing minerals occur as hematite and goethite. Traces of quartz were identified in the XRD patterns of the studied samples.

4.2.2. IR

IR patterns of iron ore samples from the Bahariya Oasis representing high quality ore (very low Mn contents), iron ores with some pyrolusite, and high-Mn samples from El Gedida and Ghorabi–Nasser without pyrolusite are shown in Table 4. All samples contain the characteristic OH stretching (νOH) and HOH bending (δOH) vibrational bands at 3417–3436 cm^{-1} and 1631–1635 cm^{-1}. These bands were reported in pure iron oxides (e.g. Hair, 1975; Verdonck et al., 1982) and pure manganese oxides (e.g. White et al., 2009). The IR bands of the studied samples at 466–478 cm^{-1} and 539–551 cm^{-1} are considered to represent hematite (e.g. Gotic and Music, 2007; Iglesias and Serna, 1985). These bands can also represent the stretching modes of the MnO_6 octahedra following the works of White et al. (2009) and Shahack-Gross et al. (1997). Stretching bands at 1022–1041 cm^{-1} and 1631–1635 cm^{-1} are due to the presence of goethite (e.g. Dixon et al., 1977) and/or the manganese oxides (e.g. Shahack-Gross et al., 1997).

4.2.3. Raman spectroscopy

Raman spectroscopy alone, or in combination with other techniques, has also been successfully applied to mineral and geological specimens (e.g. Dörfer et al., 2010; Klein et al., 2004; Rull et al., 2007). According to Ciobota et al. (2011), the main Raman bands of various manganese oxides are located in the wavenumber region 500–650 cm^{-1}, away from the wavenumber area, where goethite and hematite exhibit the strongest Raman signals (200–400 cm^1). Therefore, the identification of Mn-bearing minerals is not hindered by the presence of various iron oxides and/or oxyhydroxides. A number of Raman spectroscopy analyses were applied to the Mn-bearing minerals that occur as fine-grained cement-like materials in the iron ores of El Gedida and Ghorabi-Nassera areas to identify and differentiate between various Mn-bearing minerals. The obtained patterns (Fig. 4) can be classified into three groups: (1) a mixture of pyrochroite, cryptomelane, and manjiorite that are represented by the strong peak at approximately 640 cm^{-1} (Fig. 4A), (2) a mixture of aurorite, and romanechite that are characterized by two strong peaks at approximately 201 and 625 cm^{-1} (Fig. 4B), and (3) bixbyite that is represented by two strong peaks at approximately 215 and 271 cm^{-1} (Fig. 4C). The assignment of the Raman bands of the Mn-containing minerals is in concordance with previously reported investigations (e.g. Ciobota et al., 2011; Julien et al., 2004). Although

Table 2
Major oxides composition (wt.%) of representative samples from El Gedida and Ghorabi–Nasser iron ores that were analyzed by X-ray fluorescence (XRF).

Area	Samples	Ore type	SiO_2	TiO_2	Al_2O_3	Fe_2O_3	MnO_2	MgO	CaO	Na_2O	K_2O	P_2O_5	L.O.I	Total
El Gedida	2-14	Low-Mn iron ore	1.84	0.95	0.91	86.7	0.41	0.02	0.03	<bdl	0.02	0.05	8.8	99.8
	2-15	High-Mn iron ore	0.71	0.68	0.47	88.6	2.67	0.02	0.02	<bdl	<bdl	0.05	6.77	99.9
	1-6	High-Mn iron ore	0.49	0.04	1.62	67.9	8.79	0.81	0.20	0.54	0.07	0.07	19.6	100.2
	1-14	High-Mn iron ore	0.07	0.02	3.43	61.7	7.46	0.93	0.20	0.63	0.08	0.12	25.7	100.3
	1-15	Yellow Ocher	0.62	0.33	0.19	56.1	0.03	0.16	2.57	0.69	0.13	0.58	39.2	100.5
	1-16	Red Ocher	2.52	0.16	0.24	40.1	0.12	0.57	2.41	1.61	0.05	0.11	52.2	100.0
Ghorabi–Nasser	2-17	High-Mn iron ore	<bdl	0.32	1.28	47.3	13.9	0.46	0.34	0.84	0.07	0.14	35.3	100.0
	2-18	Red Ocher	13.7	0.33	4.72	68.2	3.58	1.39	0.76	1.02	0.68	0.64	5.09	100.0

bdl = Below detection limit.

Table 3
XRD data of the high-Mn iron ores from El Gedida and Ghorabi–Nasser areas.

Area	Sample	Ni-filtered Cu-Kα		Fe-filtered Co-Kα		No-filtered Fe-Kα	
El Gedida	2-15	2θ°	Mineral identification	2θ°	Mineral identification	2θ°	Mineral identification
		24.2	Goethite	24.8	Goethite		
		28.5	Pyrolusite	28.2	Hematite		
		33.1	Hematite	33.5	Pyrolusite		
		35.7	Hematite	39	Hematite		
		37.2	Pyrolusite	41.7	Pyrolusite		
		40.8	Hematite	43	Goethite		
		49.5	Hematite	43.8	Pyrolusite		
		54	Hematite	48.2	Pyrolusite	Not analyzed	
		56.3	Hematite	50	Pyrolusite		
		62.4	Hematite	54	Pyrolusite		
		64	Hematite	58.3	Hematite		
				63.8	Hematite		
				65	Goethite		
				66	Goethite		
				68	Hematite		
	1-6	24.2	Goethite	28.3	Hematite	30.6	Hematite
		33.1	Hematite	38.7	Hematite	38	Hematite
		35.7	Hematite	42	Hematite	41.2	Bixbyite
		40.8	Hematite	48.1	Hematite	42.3	Hematite
		49.5	Hematite	58.5	Hematite	45.6	Cryptomelane, romanechite, manjiroite, pyrochroite
		54	Hematite	64	Hematite	47	Hematite
		56.3	Hematite	68	Hematite	52.3	Hematite
		62.4	Hematite			61.6	Hematite
		64	Hematite			67.8	Hematite
	1-14	24.2	Goethite	14.7	Aurorite	16	Aurorite
		33.1	Hematite	21.6	Aurorite	23.4	Aurorite
		35.7	Hematite	28.4	Hematite	27.6	Aurorite
		40.8	Hematite	31.4	Quartz	30.6	Hematite
		49.5	Hematite	38.7	Hematite	33.7	Quartz
		54	Hematite	42	Hematite	38.1	Hematite
		56.3	Hematite	48.2	Hematite	41	Bixbyite
		62.4	Hematite	58.4	Hematite	42.3	Hematite
		64	Hematite	64	Hematite	45.4	Hematite
				68.2	Hematite	47.2	Cryptomelane, romanechite, manjiroite, pyrochroite
						52.2	Hematite
						57	Aurorite
						62.5	Hematite
						63.6	Hematite
						69.8	Hematite
Ghorabi–Nasser	2-17	24.2	Goethite	28.5		30.8	Hematite
		33.1	Hematite	38.9		38.2	Hematite
		35.7	Hematite	42		40.2	Rhodochrosite
		40.8	Hematite	48.2		41	Bixbyite
		49.5	Hematite	58.5		42.2	Hematite
		54	Hematite	64		45.4	Hematite
		56.3	Hematite	68.5		47.2	Cryptomelane, romanechite, manjiroite, pyrochroite
		62.4	Hematite			52.2	Hematite
		64	Hematite			63.8	Hematite
						70	Hematite

Mn carbonate mineral (rhodochrosite) was detected in the Ghorabi–Nasser high-Mn iron ores by XRD, no Mn carbonate minerals were detected in the Raman patterns of the studied samples. Consistent with the XRD data, pyrolusite was not identified in the obtained Raman data, although Ciobota et al. (2011) could identify it in the iron ores from Ghorabi–Nasser area using Raman spectroscopy.

4.3. Petrography and minerals chemistry

4.3.1. Petrography

Petrographic investigations and back scattered electrons (BSE) images of the high-Mn iron ores from El Gedida mine indicated that Mn-bearing minerals occur either as pyrolusite or fine-grained cement-

Table 4
Selective IR data (Wavenumber cm^{-1}) for low-Mn and high-Mn (with and without pyrolusite) iron ores from El Gedida and Ghorabi–Nasser areas.

Peak no.	El Gedida area			Ghorabi–Nasser area	Assignment	References
	2-14	2-15	1-14	2-17		
	Low-Mn iron ore	High-Mn iron ore (some pyrolusite)	High-Mn iron ore (no pyrolusite)	High-Mn iron ore (no pyrolusite)		
1	466	474	470	478	Fe–O, Mn–O	Gotic and Music (2007), Iglesias and Serna (1985),
2	539	551	543	551	Fe–O, Mn–O	White et al. (2009), Shahack-Gross et al. (1997)
3	1029	1033	1022	1041	Fe–O–H, Mn–O	Dixon et al. (1977), Shahack-Gross et al. (1997)
4	1635	1635	1635	1631	νH–O……H, Mn–O	
5	3421	3436	3417	3421	νH–O……H	Hair (1975), Verdonck et al. (1982), White et al. (2009)

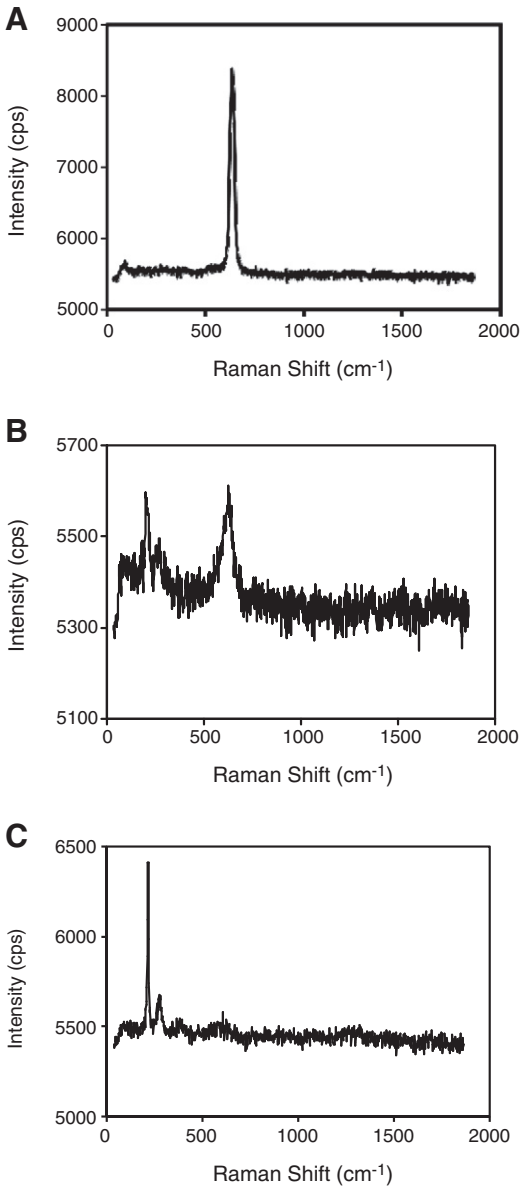

Fig. 4. Raman spectra of the Mn minerals. (A) Pattern represents pyrochroite, cryptomelane, and manjiorite minerals. (B) Pattern represents aurorite and romanechite. C) Pattern of typical bixbyite.

like materials. Pyrolusite occurs in one sample as relatively coarse-grained (up to 0.1 mm) and well-crystalline constituent between iron-bearing minerals (Fig. 5A) with prominent transverse cracks. These cracks are somewhat characteristic of this pyrolusite and were considered by Ramdohr (1956) to be contraction cracks formed during the dehydration of manganite to pyrolusite. Mn minerals that filled the interstitial spaces between grains appear as gray to dark gray fine-grained materials (Fig. 5B). Mn-rich parts inside the Fe-bearing minerals appear as light gray spots of less reflectivity compared to hematite and goethite (Fig. 5C). On the other hand, petrographic investigations and BSE images of the high-Mn iron ores from the Ghorabi–Nasser area indicated that Mn-bearing minerals occur only as cement-like of fine-grained gray to dark gray materials (Fig. 5D). Hematite and goethite are the main constituents of the studied samples of both localities. Hematite occurs as irregular grains and patches of variable sizes ranging from 50 to 200 μm (Fig. 5D), whereas goethite is characterized, in most cases, by spherical and botryoidal shapes of different sizes ranging from few microns up to100 μm (Fig. 5C). Relatively coarse-grained (up to 0.2 mm) subrounded, and monocrystalline detrital quartz grains are quite common in some of the studied samples. Dark gray to brownish gray dull patches of variable sizes are found between grains that are most probably clay minerals.

4.3.2. SEM observations

Scanning electron microscopy (SEM) observations of the same samples indicate that the hematite occurs in different morphologies. In the high-Mn sample from El Gedida mine, hematite occurs as flakes of variable sizes similar to filamentous microbial-like forms (Fig. 6A), whereas in the high-Mn sample from the Ghorabi–Nasser area, hematite occurs mainly as rod-, cocci- and bacilli-like morphologies (Fig. 6C). However, goethite occurs in both localities as clumps of small, uniformly sized globular phases with concentric internal structure (Fig. 6C). Energy dispersive spectrometer (EDS) analysis of both hematite and goethite exhibit the characteristic peaks of Mn (Fig. 6B, D and E). This can be attributed to the occurrence of Mn as very fine inclusions within the Fe-bearing minerals and/or accumulated on the active surface of Fe-oxides during the transformation of primary ferrihydrite to goethite and/or hematite. Occurrence of Mn in the structure of Fe-bearing minerals is still possible (e.g. Baron et al., 2005). However, the EDS analysis cannot confirm that precisely due to the relatively large size of beam. More precise tools such as transmission electron microscope (TEM) can give a more accurate conclusion. Except pyrolusite that occurs as coarse-grained well-crystalline and blocky crystals within the Fe-bearing minerals (Fig. 6F and G), no Mn-bearing minerals were identified by SEM.

4.3.3. EPMA elemental distribution mapping and quantitative analysis

EPMA elemental distribution mapping of the high-Mn iron ores showed compositional variations in Mn contents in the different forms of Mn-bearing minerals. In the case of Mn that occurs as active Mn and/or inclusions within the Fe-bearing minerals, Mn is found as small isolated islands inside hematite and/or goethite (Fig. 7A and B) at the expenses of Fe that occurs in lower concentrations in the high-Mn areas. Pyrolusite crystals, on the other hand, show the highest Mn contents and approximately free from Fe; there is a complete decoupling between Fe and Mn in these samples (Fig. 7C and D). The cryptocrystalline Mn-bearing minerals that occur as cement-like materials (Fig. 7E and F) are also very poor in Fe. Mn also, occasionally, found as high-Mn ooids and numerous rounded particles of various sizes within a relatively low-Mn groundmass (Fig. 7G and H). The small rounded particles display pisolitic botryoidal shapes where the rims of these botryoids are much richer in Fe than the core (Fig. 7G and H). The quantitative analyses of different Mn-bearing phases using the electron probe micro analyzer (EPMA) show compositional variations in terms of their MnO_2 contents. MnO_2 content in the hematite and goethite grains (as Mn on the active surface of Fe-bearing minerals and/or inclusions) (Table 5) ranges from 4.1 to 18.9 wt.%, which in a broad sense is consistent with the EDS analysis of the same minerals. Pyrolusite shows the highest MnO_2 contents (94.8–96.5 wt.%) and low contents of other impurities such as MgO, CaO, and Na_2O (Table 6). Mn-bearing minerals that occur mainly as fine cement-like phases showed less MnO_2 contents (average of 50 wt.%) (Tables 7 and 8) compared with pyrolusite (average of 96 wt.%). Other oxides such as MgO, CaO, and Na_2O occur in considerably high contents and show strong positive correlations with MnO_2 in the cement-like Mn-bearing minerals (Fig. 8A, B, and C). No correlations were observed between these oxides and MnO_2 in both pyrolusite and those of goethite and hematite that contain Mn as inclusion and/or accumulated on their active surfaces (Fig. 8D, E, and F). The less MnO_2 contents, the relatively high MgO, CaO, K_2O, and Na_2O, and positive correlations between MnO_2 and those oxides in the cement-like Mn-bearing minerals support the mineralogical interpretations that the cement-like Mn-bearing minerals occur as carbonate (rhodocrosite), hydrate (aurorite), and hydroxide minerals (pyrochroite) that should have less MnO_2 contents compared to pyrolusite. Also minerals such as aurorite and manjiroite contain

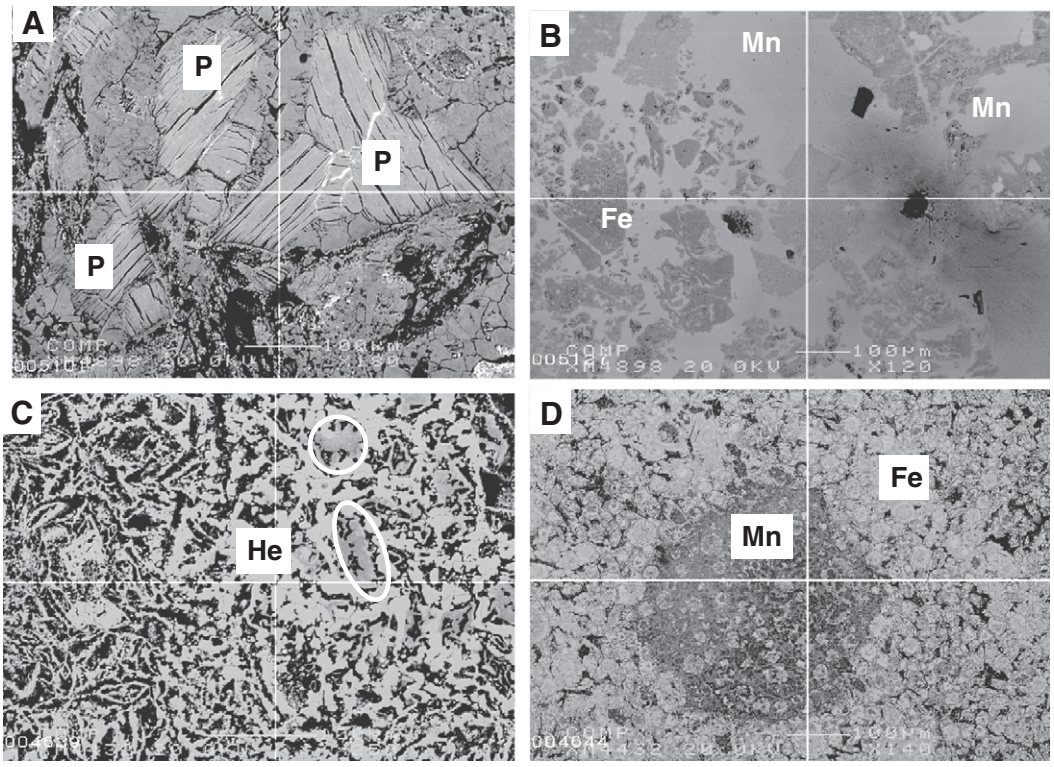

Fig. 5. BSE images of the high-Mn ores in the El Gedida and Ghorabi–Nasser iron ores. (A) Coarse-grained well crystalline pyrolusite (P) distinguished cracks. (B) Fine-grained Mn-bearing minerals (Mn) within the coarse grains of Fe-bearing minerals (Fe). (C) White circle refers to the area (gray area) where Mn occurs as inclusion or accumulates on the active surface of the hematite (He). (D) Fine-grained cement-like Mn-bearing minerals (Mn) between grains of Fe-bearing minerals (Fe) that occur as clumps of small, uniformly sized globular phases with concentric internal structure.

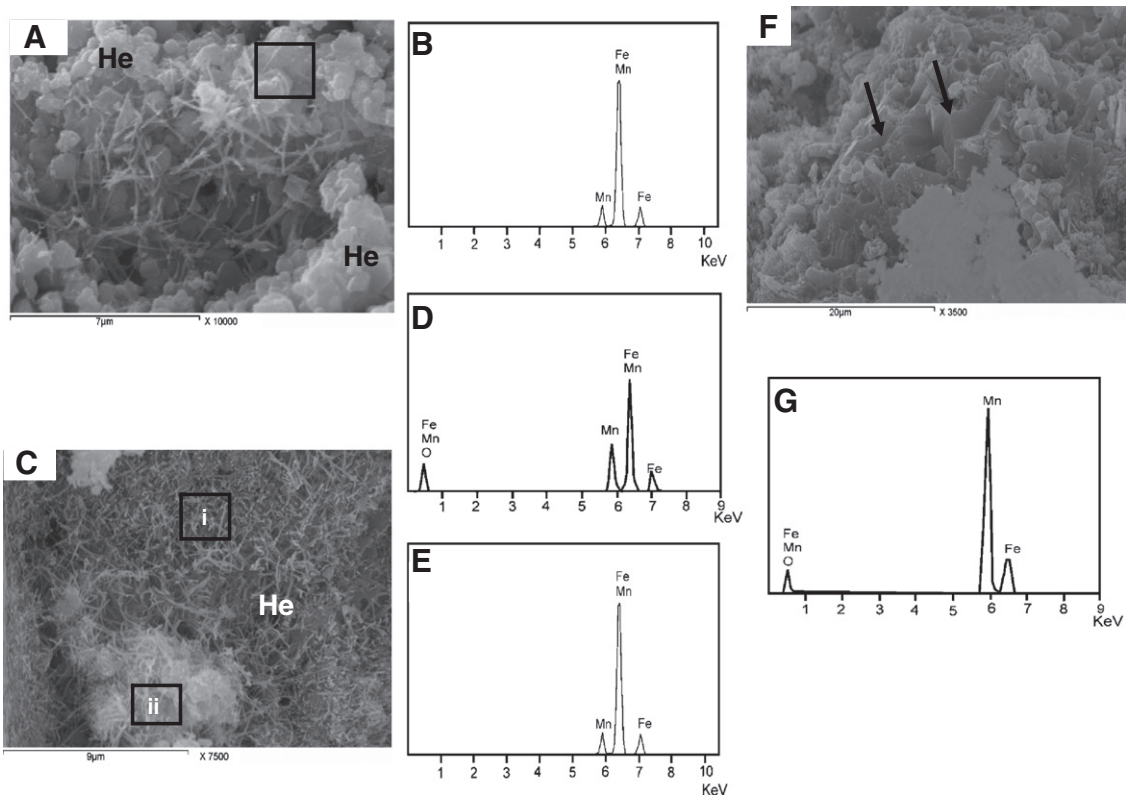

Fig. 6. SEM image of iron ores from El Gedida iron mine. (A) SEM image shows the occurrence of hematite (He) as flakes of variable sizes. (B) EDX analysis of the square area in (A) shows the occurrence of Mn in the structure of hematite. (C) SEM image of iron ores from the Ghorabi–Nasser area shows the occurrence of hematite (He) as rod-, cocci- and bacilli-like morphology. (D) and (E) EDX analyses of the squared area in (C) show the association of Mn with the hematite (i) and goethite (ii), respectively. (F) SEM image of pyrolusite that occurs as massive blocky crystals (arrows) ores from the Ghorabi–Nasser area shows the occurrence of hematite (G) EDX analysis of the pyrolusite crystals showing the predominance of Mn.

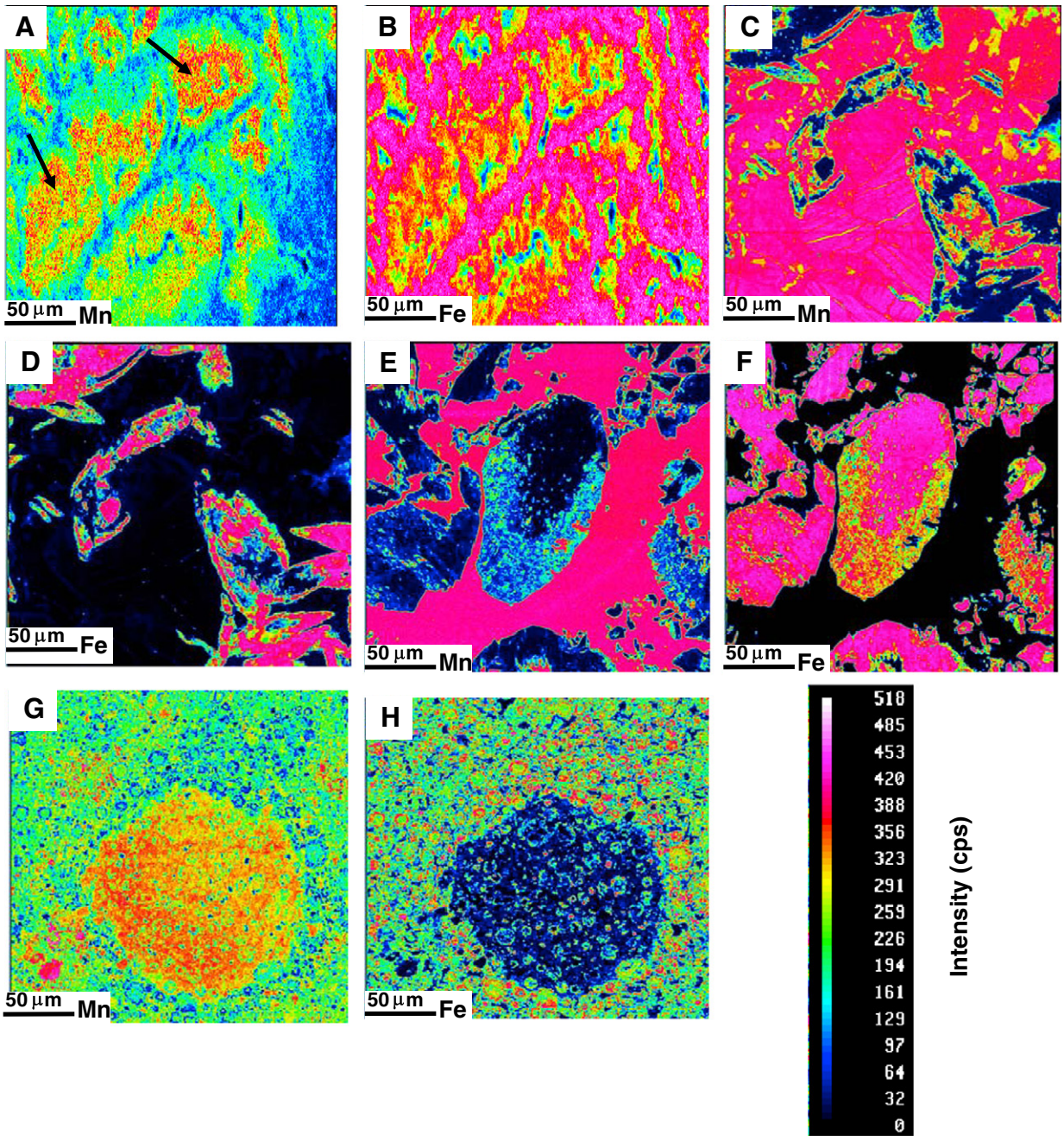

Fig. 7. EPMA elemental mapping shows the distribution of Mn and Fe in the different Mn-bearing phases. (A, B) Mn occurs as inclusions (arrows) in the hematite grains as indicated from the high concentration of Mn (reddish patches) and low contents of Fe in the inclusions areas. (C, D) Pyrolusite from El Gedida area with very high Mn concentration appeared as strong pinkish to reddish colors and low Fe content of almost black color. In the cement-like Mn-bearing phases from El Gedida and Ghorabi–Nasser areas, the high Mn content is characterized by the strong pinkish to reddish color (E and F, respectively), while the low Fe content is indicated from the almost black color (G and H, respectively).

relatively high contents of K_2O, CaO, and Na_2O, while others such as romanechite contains Ba, which was not analyzed by EPMA.

5. Discussion

5.1. Identification of Mn-bearing minerals

The identification of Mn-bearing minerals in the Bahariya iron ores was a problem in previous studies to the extent that Nakhla and Shehata (1967) did not report any Mn-bearing minerals although they reported high MnO contents (12.8%) in their chemical analysis. Salama et al. (2012) indicated that the manganese minerals are only identifiable by Raman Spectroscopy (spot analyses) and it is difficult to make a quantitative statement about their occurrences. In this study, more than one mineralogical analytical tool was implemented to find the best way to identify and distinguish between various manganese minerals including IR, Raman spectroscopy and XRD with different X-ray sources. The IR patterns of low-Mn and high-Mn (with and without pyrolusite) iron ores are almost the same. This is because the IR patterns of Fe-bearing and Mn-bearing minerals (mostly oxides) in the studied samples are the same. Therefore, IR analytical tool cannot be used to identify or differentiate between the Mn-

Table 5
Representative microprobe analysis (wt.%) of hematite from the Bahariya iron ores in which Mn occurs as inclusions and/or accumulated on the active surface of the hematite (Sample # 1-6 represents the high-Mn iron ores from El Gedida area).

No.	SiO_2	Al_2O_3	Fe_2O_3	MnO_2	MgO	CaO	Na_2O	K_2O	Total
51	2.07	0.21	79.66	8.18	0.65	0.28	0.10	bdl	91.15
52	2.03	0.11	79.58	7.64	0.69	0.27	0.09	bdl	90.42
53	1.51	1.69	66.33	18.93	2.06	0.44	0.10	0.02	91.08
54	1.35	1.33	64.27	18.09	2.55	0.36	0.11	0.02	88.06
55	1.48	1.47	66.20	16.90	2.59	0.41	0.11	bdl	89.18
56	2.10	0.12	81.20	6.57	0.73	0.26	0.07	0.02	91.08
57	1.31	1.15	70.36	18.92	2.75	0.37	0.07	bdl	94.92
59	2.80	1.27	82.85	4.96	0.54	0.31	0.04	bdl	92.84
61	1.73	1.97	68.51	16.77	1.95	0.53	0.06	0.03	91.56
62	2.32	0.18	81.60	6.86	0.64	0.25	0.04	bdl	91.90
63	3.11	2.10	79.89	6.11	1.96	0.45	0.05	bdl	93.72
64	3.11	1.78	79.87	4.09	2.79	0.37	0.05	bdl	92.08
65	2.64	0.60	82.28	7.31	0.51	0.26	0.13	0.03	93.82
66	2.59	0.55	81.65	7.54	0.54	0.26	0.10	0.02	93.25
67	2.41	0.44	80.04	8.97	0.52	0.28	0.14	0.04	92.86
68	2.49	0.45	80.49	8.02	0.50	0.26	0.10	0.03	92.36
69	2.45	0.54	81.34	8.23	0.57	0.27	0.08	bdl	93.50

bdl = Below detection limit.
TiO_2 contents are below the detection limit in all analyses.

and Fe-bearing minerals or between the Mn-bearing minerals, themselves, in the Bahariya iron ores.

Pyrolusite is the only Mn-bearing mineral that could be identified in the XRD patterns of Ni-filtered Cu-Kα, Fe-filtered Co-Kα, and non-filtered Fe-Kα run, while aurorite was identified in the XRD patterns of Fe-filtered Co-Kα run as well as the XRD patterns of non-filtered Fe-Kα runs. On the other hand, other Mn-bearing minerals such as bixbyite, cryptomelane, aurorite, romanechite, manjiroite, pyrochroite, rhodochrosite, andrhodonite, which occur mainly as fine-grained cement-like constituents, appeared only in the non-filtered Fe-Kα run. This could be due to the relatively high crystallinity of pyrolusite and the low crystallinity of other Mn-bearing minerals that occurs mainly as cement-like materials of fine-grained phases. Moreover, most of the identified Mn-bearing minerals in the studied samples are overlapped, which makes it difficult to confirm the occurrence of all minerals in the studied ores. Absence of Mn-bearing minerals in the Ni-filtered Cu-Kα and Fe-filtered Co-Kα runs can explain why they were not reported in some of the previous studies (e.g. Nakhla and Shehata (1967). These studies used the Cu-Kα and/or Co-Kα to analyze the high-Mn iron ores. Thus the application of XRD techniques to study the mineralogy of high-Mn iron ores in the Bahariya Oasis should be treated carefully and a suitable X-ray source (non-filtered Fe-Kα) should be used to get diffraction peaks for manganese minerals.

Table 6
Representative microprobe analysis (wt.%) of pyrolusite from El Gedida iron ores (Sample # 2-15 represents the high-Mn iron ores from El Gedida area).

No.	SiO_2	Al_2O_3	Fe_2O_3	MnO_2	MgO	CaO	Na_2O	K_2O	Total
71	0.09	0.06	0.63	95.94	0.03	0.13	0.10	0.02	96.99
73	0.21	0.10	0.75	96.03	0.05	0.18	0.10	0.20	97.63
74	0.30	0.10	0.94	95.68	0.06	0.19	0.12	0.06	97.44
75	0.20	0.14	0.66	96.11	0.08	0.12	0.16	0.32	97.83
79	0.30	0.06	0.96	95.48	0.13	0.24	0.16	0.11	97.45
80	0.14	0.03	0.62	95.90	0.12	0.25	0.17	0.08	97.29
82	0.36	0.39	0.90	96.20	0.12	0.21	0.11	0.06	98.34
83	0.19	0.20	0.47	94.83	0.02	0.08	0.06	0.12	95.99
84	0.36	0.15	0.47	96.47	0.05	0.14	0.10	0.06	97.81
87	0.14	0.03	0.35	96.19	0.08	0.15	0.04	0.03	97.02
89	0.23	0.09	0.42	95.92	0.04	0.15	0.09	0.18	97.14

TiO_2 contents are below the detection limit in all analyses.

Table 7
Representative microprobe analysis (wt.%) of hydrous Mn-bearing minerals that occur as cryptocrystalline cement-like phases in El Gedida high-Mn iron ores (Sample # 1-14).

No.	SiO_2	TiO_2	Al_2O_3	Fe_2O_3	MnO_2	MgO	CaO	Na_2O	K_2O	Total
4	1.03	0.06	0.82	41.68	46.35	0.63	0.48	0.60	0.15	91.81
5	0.44	0.11	0.73	9.66	69.13	1.79	0.94	0.89	0.78	84.47
6	2.49	0.15	1.83	3.41	69.59	1.85	0.92	1.03	1.14	82.39
7	1.51	0.09	0.61	77.92	11.43	0.26	0.40	0.16	0.07	92.47
8	5.42	0.12	2.83	3.71	62.92	2.73	0.82	0.98	1.60	81.13
9	1.70	0.07	0.76	74.86	13.84	0.31	0.37	0.14	0.11	92.15
10	0.12	0.06	0.82	1.10	74.44	3.00	0.63	0.91	1.42	82.50
11	0.36	0.14	0.72	12.82	65.54	2.28	0.74	0.98	1.05	84.61
12	1.30	0.07	0.76	51.05	34.49	0.94	0.58	0.45	0.41	90.04
13	4.63	0.16	2.41	4.89	66.05	1.99	0.93	0.96	1.64	83.65
15	0.44	0.10	0.71	0.54	8.96	1.94	0.89	0.98	0.88	85.16
16	1.82	0.07	0.82	12.93	66.28	0.43	0.36	0.29	0.14	85.13
17	2.00	0.06	0.63	73.61	14.64	0.27	0.30	0.22	0.08	92.16
18	1.53	0.11	0.79	81.27	8.81	0.92	0.40	0.52	0.27	93.64
19	0.13	0.06	0.68	63.91	23.05	2.27	0.61	1.12	1.48	91.49
20	0.13	0.06	0.68	0.88	74.03	2.93	0.70	1.01	1.46	81.26
21	1.09	0.08	0.74	0.90	75.25	1.03	0.59	0.49	0.46	83.12
22	1.05	0.06	0.73	45.42	37.23	0.55	0.46	0.40	0.15	87.13
23	1.50	0.13	1.22	44.58	45.50	1.84	0.89	0.83	0.91	93.48
24	0.65	bdl	0.12	5.68	70.21	0.13	0.05	0.10	bdl	83.21
25	0.59	bdl	0.12	88.05	4.56	0.14	0.04	0.11	bdl	93.67
26	0.28	0.33	0.98	89.33	1.85	0.79	0.88	0.63	0.32	92.18
27	0.27	0.29	0.97	0.19	79.13	0.92	0.98	0.68	0.31	83.51
28	0.26	0.35	0.93	0.17	78.83	0.95	0.87	0.72	0.32	83.42
29	0.30	0.36	0.98	0.22	80.58	1.60	0.99	0.65	0.32	85.20

bdl = Below detection limit.

Although the Raman spectroscopy analysis shows an overlapping in the identified Mn minerals, bixbyite shows a unique pattern. Also aurorite and romanechite minerals showed a distinguished pattern compared to other minerals. Therefore, a combination of X-ray diffraction analysis using non-filtered Fe-Kα radiations and Raman spectroscopy could be the best way to identify and distinguish between different Mn minerals.

Table 8
Representative microprobe analysis (wt.%) of hydrous Mn-bearing minerals that occur as cryptocrystalline cement-like phases in the Ghorabi–Nasser high-Mn iron ores (Sample # 2-17).

No.	SiO_2	TiO_2	Al_2O_3	Fe_2O_3	MnO_2	MgO	CaO	Na_2O	K_2O	Total
4	1.03	0.06	0.82	41.68	46.35	0.63	0.48	0.60	0.15	91.81
5	0.44	0.11	0.73	9.66	69.13	1.79	0.94	0.89	0.78	84.47
6	2.49	0.15	1.83	3.41	69.59	1.85	0.92	1.03	1.14	82.39
7	1.51	0.09	0.61	77.92	11.43	0.26	0.40	0.16	0.07	92.47
8	5.42	0.12	2.83	3.71	62.92	2.73	0.82	0.98	1.60	81.13
9	1.70	0.07	0.76	74.86	13.84	0.31	0.37	0.14	0.11	92.15
10	0.12	0.06	0.82	1.10	74.44	3.00	0.63	0.91	1.42	82.50
11	0.36	0.14	0.72	12.82	65.54	2.28	0.74	0.98	1.05	84.61
12	1.30	0.07	0.76	51.05	34.49	0.94	0.58	0.45	0.41	90.04
13	4.63	0.16	2.41	4.89	66.05	1.99	0.93	0.96	1.64	83.65
15	0.44	0.10	0.71	12.93	66.28	1.94	0.89	0.98	0.88	85.13
16	1.82	0.07	0.82	73.61	14.64	0.43	0.36	0.29	0.14	92.16
17	2.00	0.06	0.63	81.27	8.81	0.27	0.30	0.22	0.08	93.64
18	1.53	0.11	0.79	63.91	23.05	0.92	0.40	0.52	0.27	91.49
19	0.13	0.06	0.68	0.88	74.03	2.27	0.61	1.12	1.48	81.26
20	0.13	0.06	0.68	0.90	75.25	2.93	0.70	1.01	1.46	83.12
21	1.09	0.08	0.74	45.42	37.23	1.03	0.59	0.49	0.46	87.13
22	1.05	0.06	0.73	44.58	45.50	0.55	0.46	0.40	0.15	93.48
23	1.50	0.13	1.22	5.68	70.21	1.84	0.89	0.83	0.91	83.21
97	1.72	0.06	0.82	55.96	29.60	0.69	0.39	0.45	0.21	89.90
98	1.64	0.07	0.73	59.72	25.04	0.54	0.32	0.37	0.19	88.61
99	1.28	0.08	0.85	40.63	39.53	1.11	0.50	0.63	0.37	85.01
100	0.51	0.06	0.80	12.45	72.75	2.19	0.66	1.12	0.73	91.26
101	0.22	0.06	0.67	1.41	78.99	2.12	0.74	1.10	0.95	86.26
102	0.38	0.03	0.30	6.59	77.82	2.42	0.41	1.29	0.78	90.02
103	0.94	0.02	0.50	41.41	38.18	0.55	0.38	0.35	0.07	82.39
104	0.96	0.06	0.78	36.41	40.42	0.71	0.45	0.47	0.17	80.43
105	0.66	0.05	0.76	25.34	51.61	1.68	0.60	0.64	0.26	81.61
106	0.30	0.05	0.73	1.48	78.65	2.18	0.68	1.13	0.95	86.15

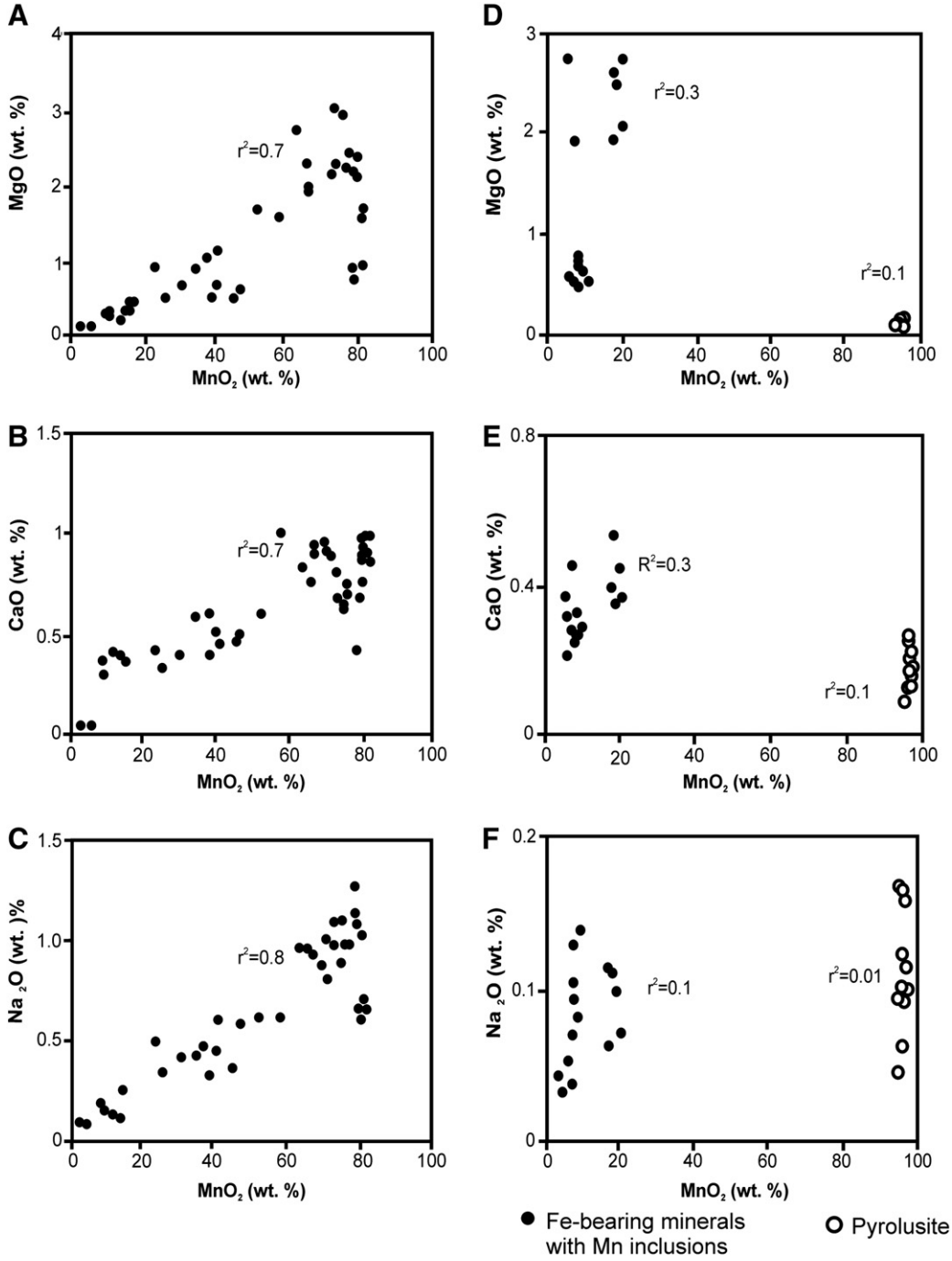

Fig. 8. Binary plot of MnO_2 vs. MgO, CaO, and Na_2O in the different Mn-bearing phases. The positive correlations between MnO_2 and MgO, CaO, and Na_2O (A, B, and C, respectively) in the cement-like Mn-bearing phases in both El Gedida and Ghorabi–Nasser iron ores suggest the occurrence of these oxides in the structure of Mn-bearing minerals. While, the lack of correlations between MnO_2 and MgO, CaO, and Na_2O (D, E, and F, respectively) in the pyrolusite and hematite with Mn as inclusions and/or accumulated on its active surface is suggestive for the occurrence of these oxides in different phase(s).

5.2. Forms of Mn in the Bahariya high-Mn iron ores

Mineralogical and petrographic investigations of the high-Mn iron ores from the Bahariya Oasis suggest three modes of occurrence for Mn in these ores. (1) Mn as inclusions and/or accumulated on the active surface of the hematite and goethite appeared as irregular spots of different sizes in the Mn-distribution map. The inclusions could be a complete chemical substitution of iron by manganese in the Fe-bearing minerals and/or mechanical replacement of Mn-bearing mineral(s) of goethite and hematite. Accumulation of Mn-oxide on the active surfaces of Fe-bearing minerals can be explained by the oxide surface catalysis model advocated by Morgan (2005). Metal-oxide surfaces are able to accelerate Mn(II) oxidation by redox reactions (e.g. hematite, goethite, lepidocrocite, and manganese dioxide) (Davies and Morgan, 1989; Sung and Morgan, 1981; Wilson, 1980). According to Polgári et al. (2012a), pores of stromatolite-like cherty Fe–Mn-oxide in the Mn-carbonate ore deposit in the Úrkút area, Hungary were filled by Mn-oxide minerals around the reactive surfaces of Fe oxides. (2) Well-crystalline and coarse-grained pyrolusite, which was identified only in El Gedida iron ores. According to Ramdohr (1956), pyrolusite can be formed by the dehydration of manganite. The present study did not show any evidence for the

formation of pyrolusite after manganite since no manganite was reported in the mineralogical composition of the studied samples. (3) Mn as cement-like materials that fill the interstitial spaces between Fe-bearing minerals with sharp contact. XRD analysis using Fe-Kα radiation indicates the presence of Mn-bearing minerals of this type as a mixture of bixbyite, cryptomelane, aurorite, romanechite, manjiroite, pyrochroite, and rhodochrosite. Occurrence of such Mn-bearing minerals as cement between Fe-bearing minerals suggests a precipitation of the former after the formation of the later due to the relatively higher solubility of Mn compared to Fe. Mn is more soluble than Fe and can be retained in the solution for a long time until finding a reducing barrier to be precipitated later between the already formed Fe-bearing minerals (e.g. Hein et al., 2008; Krauskopf, 1957; Mohapatra et al., 2009; Nicholson, 1992). The small size (about 1 μm) of Mn-bearing minerals has been used by Polgári et al. (2012a) to indicate microbial activity in the Jurassic Mn-carbonate ore deposit in the Úrkút area, Hungary. Therefore, the very fine-grained size of oxide and hydroxide minerals of the studied high-Mn iron ores supports the petrographic evidences of microbial origin of these high-Mn iron ores.

SEM and EPMA investigations also indicated the association of Fe with the Mn-bearing minerals. Quantitative analysis indicated that the Fe_2O_3 contents in the Mn minerals that occur as cement-like minerals vary between 0.2 and 11 wt.%. Iron in these minerals can occur as inclusions and/or in the structure of some of these minerals such as bixbyite that contains from 14 to 50 wt.% of Fe_2O_3 (e.g., Geller, 1971).

5.3. Origin of Mn

The origin of iron ores in the Bahariya Oasis has been a matter of scientific discussions for a long time. Seven possible sources of iron in these ores were discussed in the previous literatures. (1) Direct precipitation of iron from a shallow water lagoonal and lacustrine environment and replacing the underlying middle Eocene limestone (e.g., Akkad and Issawi, 1963; Attia, 1950; El Shazly, 1962). (2) Lateritization and karstification of host limestone (e.g., El Aref and Lotfy, 1985). (3) Weathering of the overlying glauconite of the Hamra Formation (e.g. Baioumy and Hassan, 2004; Dabous, 2002; El Sharkawi et al., 1984). (4) Iron has been oxidized and leached from the sandstone of the Nubia aquifer by upward-moving groundwater and deposited in the overlying pre-existing limestone (e.g. Dabous, 2002). (5) Iron sourced from the underlying basement igneous and metamorphic rocks (e.g. Hussein, 1990). (6) Metasomatic replacement of the underlying limestone by hydrothermal solutions (e.g., Basta and Amer, 1969; El Sharkawi et al., 1984; Nakhla, 1961). (7) Volcanogenic source (e.g., Tosson and Saad, 1974). From the above-mentioned review, a fundamental question with regard to the origin and source of Fe and Mn in the studied deposits should be definitely answered: were the deposits formed by descending solutions such as direct precipitation from the seawater, lateritization and karstification of host limestone, and leaching of overlying glauconite and then replacing the preexisting carbonates, or by ascending solutions including hydrothermal solutions, volcanic eruption, or leaching of the underlying sandstones of the Bahariya Formation and/or the basement rocks. The following part of this discussion tries to answer this question through the data obtained from the geological, petrographic, mineralogical, and geochemical investigations on the high-Mn iron ores.

Geologically, iron ores including Mn-rich iron ores occur as bedded and stratiform ores that characterize the sedimentary origin of the deposits (Nicholson, 1992), not as veins or stratabound that characterizes the hydrothermal origin (e.g. Basta and Saleeb, 1971). Assuming that Fe and Mn were derived from the same source, Krauskopf (1957), Nicholson (1992), Hein et al. (2008), and Mohapatra et al. (2009), indicated that Mn and Fe in solutions are characteristically fractionated to produce high or low Mn/Fe ratios, based on which one is more dominant. If the Mn and iron were sourced by descending (supergene) solutions, due to the higher solubility of Mn compared to Fe, the Fe could be precipitated first in the upper part of the succession close to the source of elements, and then Mn will be precipitated in the lower part relatively far from the source. If Mn was produced by ascending (hypogene) solutions, it would be precipitated upward, leaving Fe in the lower part of the succession. The occurrence of high-Mn iron ores in the base of the iron deposits of the Bahariya Oasis overlain by the low-Mn iron ores (e.g. Salama et al., 2012) suggested a descending (supergene) solution as a source of Mn and Fe in the studied deposits.

As a tool in recognizing the genesis of manganese deposits, mineralogy has been used by various researchers for a long time. In most cases, however, a diagnostic mineral assemblage has been hampered by the weathering and metamorphism of the primary ore deposit, and mineralogical variations between two or more deposits formed in similar environments (Nicholson, 1992; Ostwald, 1992; Rona, 1978). According to Nicholson (1992), bixbyite, braunite, hausmannite, huebnerite, jacobsite, and pyrochroite occur predominantly only in hydrothermal deposits, whereas chalcophanite, coronadite, crednerite, delta-MnO_2, groutite, hollandite, lithiophorite, manganite, nsutite, quenselite, ramsdellite, romanechite, todorokite, and woodruffite are generally of supergene origin. Fan and Yang (1999) classified the manganese deposits in China into six types based on origin and subsequent modifications: (1) sedimentary, (2) volcanic-sedimentary, (3) metamorphosed, (4) hydrothermally modified, (5) hydrothermal, and (6) supergene. Sedimentary deposits are characterized by manganese carbonate minerals (e.g. rhodochrosite, Ca rhodochrosite, Ca–Mg rhodochrosite, Fe rhodochrosite) and manganese oxide and hydroxide minerals (e.g. manganite, manganosite and chambersite), whereas supergene deposits are characterized only by manganese oxides (e.g. pyrolusite, ramsdellite, psilomelane and vernadite). Volcanic-sedimentary, metamorphosed, endogenic and hydrothermal deposits have various and complex mineral compositions and are mostly composed of Mn oxides and Mn silicates. Applying the classification of Nicholson (1992), the Bahariya iron ores have a mixture of hydrothermal-based minerals (i.e. bixbyite, pyrochroite, and braunite) and hydrogeneous-based minerals (i.e. romanechite). However, following the classification of Fan and Yang (1999), a supergene origin of Mn in the studied ores is probable since the Mn-bearing minerals are mainly a mixture of manganese oxides and hydroxides. Roy (1992) considered that in manganese deposits formed from ascending hydrothermal solutions there is a zonal arrangement of minerals: in the deepest part of the epithermal zone rhodonite, rhodochrosite, and alabandite (with Mn^{2+}) are present, followed upwards by hausmannite, bixbyite, and braunite (Mn^{2+} and Mn^{4+}), and ultimately, in the uppermost parts, by psilomelane, cryptomelane, pyrolusite, etc. (mainly Mn^{4+}). In the current study, no such zonal arrangement of Mn-bearing minerals was found supporting the geological interpretation that the studied deposits were derived from descending (supergene) solutions. High-Mn grains occur in many cases, especially in the Ghorabi–Nasser area, in botryoidal shapes that can represent colloidal supergene Mn-oxy-hydroxides. In addition, SEM investigations of the high-Mn iron ores show evidence of microbial role in the formation of high-Mn iron ores such as spherical, elliptical, and filamentous textures (e.g. Polgári et al., 2012a,b). According to Polgári et al. (2012a), filamentous Fe oxide represents suboxic conditions, whereas the high-Mn parts may reflect oxic subconditions in the Fe ores.

Geological and mineralogical data suggest supergene descending solutions as possible source of Mn in the Bahariya iron ores. Three possibilities can be suggested for the supergene descending solutions in the studied area including the direct precipitation from the seawater, leaching of Fe from the overlying glauconites, and/or karstification of the host Naqb limestone. Due to the low dissolved Fe (~3 ppb) and Mn (~4 ppb) contents in the seawater and absence of nodular texture in the studied iron ores, direct precipitation of Fe and Mn from the seawater in the Bahariya iron ores cannot be considered. Formation of high

Mn iron ores from the weathering of the overlying glauconites also requires high Mn contents in these glauconites. The MnO_2 contents in the glauconites of the overlying Hamra Formation range from 0.02 to 0.3 wt.% (Boulis, personal communications), which makes this assumption inapplicable. Formation of high-Mn iron ores by the karstification of host limestone also requires high Mn contents in the precursor limestone (e.g. Gutzmer and Beukes, 1998). No data are available about the chemical composition of the Naqb limestone to examine the possibility of this limestone as a source of the Mn in the studied iron ores. Therefore, detailed geochemical investigations on the Bahariya iron ores and host limestone are recommended for future research work to clarify the source and origin of Mn and Fe in these ores. The geochemistry of trace and rare earth elements in the Mn deposits are widely used to distinguish between different types of these deposits (e.g. Boyd and Scott, 1999; Hewett et al., 1963; Nicholson, 1992).

5.4. Implications of the present study for Mn reduction and removal

Iron ores from the Bahariya Oasis are currently the main feedstock for the production of steel by Egyptian Company for Steel (ECS). The high contents of Mn in some of these deposits represent one of the major problems related to the utilization of these deposits. High-Mn iron ores are usually excluded from the ores charged to the production line. It means that a large quantity of the deposits is not utilized. In addition, the ore reserves are depleted due to continuous production. For this reason, the utilization of Mn-rich ores should be considered and at least blend some of them with high quality ores. One possibility to utilize the high-Mn ores is to separate Fe-bearing minerals from the Mn-bearing minerals by magnetizing reduction (e.g. Dean and Davis, 1941; El Geassy et al., 2008; Jacobs, 1970). The previous attempts for the beneficiation of the Egyptian iron ores from Bahariya Oasis assumed the occurrence of Mn as Mn-bearing minerals such as pyrolusite (e.g. El Geassy et al., 2008). None of these studies considered or assumed the accumulation of Mn on the active surfaces of hematite and goethite or as inclusions or as fin-grained cement-like materials of Mn oxides and hydroxides.

The present study revealed the occurrence of Mn in various forms in the high-Mn iron ores from the Bahariya Oasis. The reduction behavior could be different from one form to the other. For example, the reduction and separation of Mn that accumulates on the active surfaces of Fe-bearing minerals are expected to be difficult since Mn is much stocked to the surfaces of these minerals. Mn as inclusions needs grinding the ores to very fine grain-size, which increase the costs of beneficiation process. However, occurrence of Mn as pyrolusite could be the easiest form for separation. Pyrolusite reported in the studied samples ranges in size between 0.1 and 0.25 mm. Therefore, detailed petrographic and mineralogical characterizations of high-Mn iron ores are important before starting the beneficiation and/or reduction processes of high-Mn iron deposits.

Ferromanganese alloy is made by heating a mixture of the oxides MnO_2 and Fe_2O_3, with carbon (e.g. Ghafarizadeh et al., 2011). The high Mn contents, especially in the Ghorabi–Nasser iron ore and occurrence of Mn as inclusions and on the active surfaces of the Fe-bearing minerals would suggest a possible utilization of the high-Mn iron ores to produce ferromanganese alloys as an additional application of the iron ores in the Bahariya Oasis along with the steel production from low-Mn iron ores.

6. Conclusions

High-Mn iron ores of economic significance from the Bahariya Oasis were subjected to comprehensive petrographic, mineralogical, and geochemical investigations to examine the modes of occurrence of Mn and its origin. Mn occurs as inclusions and/or accumulated on the active surfaces of the hematite and goethite grains, coarse-grained and well crystalline pyrolusite, and cement-like minerals that fill the interstitial spaces between Fe-bearing minerals. The mineralogy of Mn-bearing minerals is found as a mixture of Mn oxides and hydroxides such as bixbyite, cryptomelane, aurorite, romanechite, manjiroite, and pyrochroite. Mn carbonate mineral (rhodochrosite) was detected only in the Ghorabi–Nasser iron ores.

A supergene origin by descending solution was suggested as a possible origin of the studied iron ores based on the occurrence of high-Mn deposits at the base of the succession overlain by the low-Mn iron ores and predominance of hydrous Mn-phases in botryoidal shapes. Microbial contribution to the origin of high-Mn iron ores of the Bahariya Oasis can be suggested from the small size of Mn-bearing minerals as well as the spherical, elliptical, and filamentous shapes of microbial fossils in the Fe-bearing minerals.

The results obtained here recommend a combination of X-ray diffraction analysis using non-filtered Fe-Kα radiations and Raman spectroscopy to identify and distinguish between different manganese minerals. Detailed mineralogical and petrographic investigations of each patch of the deposits are important before the ore processing due to the variation in the mineralogy and mode of occurrence of the Mn-bearing minerals in the iron ore deposits of the Bahariya Oasis from area to the other. In addition, the high Mn contents, especially in the Ghorabi–Nasser iron ore and occurrence of Mn as inclusions and/or on the active surfaces of the Fe-bearing minerals are suggestive for the possible utilization of the high-Mn iron ores in ferromanganese alloys production.

Acknowledgments

The authors would like to thank Prof. S. Arai, Kanazawa University, Japan for providing the Raman spectroscopy and EPMA elemental distribution mapping facilities.

References

Akkad, S.E., Issawi, B., 1963. Geology and iron ore deposits Bahariya Oasis. Geological Survey of Egypt, Paper 18, p. 300.
Attia, M.I., 1950. The geology of the iron-ore deposits of Egypt. Geological Survey of Egypt, Paper 7, p. 34.
Atui, L., Ryzhonkov, D.I., Sorin, S.B., Drozdov, N.N., 1999. Theory of metallurgical processes: joint reduction of oxide mixtures containing Fe_2O_3, MnO_2, and NiO with solid carbon. Steel Transl. 29, 47–49.
Baioumy, H.M., Hassan, M.S., 2004. Authigenic halloysite from El Gedida iron ores, Bahariya Oasis, Egypt: characterization and origin. Clay Miner. 39, 207–217.
Baron, V., Gutzmer, V., Rundlöf, H., Tellgren, R., 2005. Neutron powder diffraction study of Mn-bearing hematite, α-$Fe_{2-x}Mn_xO_3$, in the range $0 \le x \le 0.176$. Solid State Sci. 7, 753–759.
Basta, E., Amer, H., 1969. El Gedida iron ores and their origin, Bahariya Oases, Egypt. Econ. Geol. 64, 424–444.
Basta, E.Z., Saleeb, W.S., 1971. Elba manganese ores and their origin, South-eastern Desert, U.A.R. Mineral. Mag. 38, 235–244.
Boyd, T., Scott, S.D., 1999. Two-XRD-line ferrihydrite and Fe–Si–Mn oxyhydroxide mineralization from Franklin Seamount, western Woodlark Basin, Papua New Guinea. Can. Mineral. 37, 973–990.
Catuneanu, O., Khalifa, M.A., Wanas, H.A., 2006. Sequence stratigraphy of the Lower Cenomanian Bahariya Formation, Bahariya Oasis, Western Desert, Egypt. Sediment. Geol. 190, 121–137.
Ciobota, V., Salama, W., Tarcea, N., Rösch, P., El Aref, M., Gaupp, R., Popp, J., 2011. Identification of minerals and organic materials in Middle Eocene ironstones from the Bahariya Depression in the Western Desert of Egypt by means of micro-Raman spectroscopy. J. Raman Spectrosc. 43, 405–410.
Corona-Esquivel, R., Ortega-Gutiérrez, F., Reyes-Salas, M., Lozano-Santacruz, R., Miranda-Gasca, M.A., 2000. Mineralogical study of the La Hueca Cretaceous iron-manganese deposit, Michoacan, Southwestern Mexico. Rev. Mex. Cienc. Geol. 17, 143–153.
Dabous, A.A., 2002. Uranium isotopic evidence for the origin of the Bahariya iron deposits, Egypt. Ore Geol. Rev. 19, 165–186.
Davies, S.H.R., Morgan, J.J., 1989. Manganese (II) oxidation kinetics on metal oxide surfaces. J. Colloid Interface Sci. 129, 63–77.
Dean, R.S., Davis, C.W., 1941. Magnetic Separation of Minerals: United States Bureau of Mines Bulletin, p. 425.
Dixon, J.B., Weed, S.B., Dinauer, R.C., 1977. Minerals in Soil Environments Soil Science Society of America, Madison, Wis, p. 212.
Dörfer, T., Schumacher, W., Tarcea, N., Schmitt, M., 2010. Quantitative mineral analysis using Raman spectroscopy and chemometric techniques. J. Raman Spectrosc. 41, 684–689.

El Aref, M.M., Lotfy, Z.H., 1985. Genetic karst significance of the iron ore deposits of El Bahariya Oasis, Western Desert, Egypt. Ann. Geol. Surv. Egypt 15, 1–30.
El Aref, M.M., ElSharkawi, M.A., Khalil, M.A., 1999. The geology and genesis of stratabound to stratiform Cretaceous–Eocene iron ore deposits of El Bahariya Region, Western Desert, Egypt. Proceedings of the International Conference on Geology of the Arab World (GAW4), pp. 450–475.
El Bassyony, A.A., 1970. Geology of the Area between Gara El Hamra, Ghard El Moharik and El Harra Area, Ba-hariya Oases, Egypt. M. Sc. Thesis, Cairo University. Pp 98.
El Bassyony, A.A., 2000. Geological Setting and Origin of El Harra Iron Ores, Bahariya Oases, Western Desert, Egypt. Ann. Geol. Surv. Egypt 23, 213–222.
El Bassyony, A.A., 2005. *Bahariya teetotumensis* n. gen. n. sp. from the Middle Eocene of Egypt. Rev. Paléobiol. Genève 24, 319–329.
El Geassy, A., Nasr, M.I., Yousef, M.A., Khedr, M.H., Bahgat, M., 2008. Behavior of manganese oxides during magnetising reduction of Baharia iron ore by $CO–CO_2$ gas mixture. Ironmak. Steelmak. 27, 117–126.
El Sharkawi, M.A., Higazi, M.M., Khalil, N.A., 1984. Three genetic iron ore dikes of iron ores at El Gedida mine, Western Desert, Egypt Geological Society of Egypt. 21st Annual Meeting, Cairo, Egypt, p. 68.
El Shazly, E.M., 1962. Report on the results of drilling in the iron ore deposit of Gebel Ghorabi–Nasser, Bahariya Oasis, Western Desert. Geological Survey of Egypt. Paper 17, p. 25.
Fan, D., Yang, P., 1999. Introduction to and classification of manganese deposits of China. Ore Geol. Rev. 15, 1–13.
Geller, S., 1971. Structures of a-Mn_2O_3, $(Mn_{0.983}Fe_{0.017})_2O_3$ and $(Mn_{0.37}Fe_{0.63})_2O_3$ and relation to magnetic ordering. Acta Crystallogr. 27, 821–828.
Ghafarizadeh, B., Rashchi, F., Vahidi, E., 2011. Recovery of manganese from electric arc furnace dust of ferromanganese production units by reductive leaching. Miner. Eng. 224, 174–176.
Gotic, M., Music, S., 2007. Mossbauer, FT-IR and FE SEM investigation of iron oxides precipitated from $FeSO_4$ solutions. J. Mol. Struct. 834–836, 445–453.
Gutzmer, J., Beukes, N.J., 1998. The manganese formation of the Neoproterozoic Penganga Group, India, revision of an enigma. Econ. Geol. 93, 1091–1102.
Gutzmer, J., Beukes, N.J., 2002. Iron and manganese ore deposits: mineralogy, geochemistry and economic geology. Encyclopaedia of Life Support Systems, UNESCO, Section 5.15.6.2. (online at www.eolss.net).
Hair, M.L., 1975. Hydroxyl-groups on silica surface. J. Non-Cryst. Solids 19, 299–309.
Hein, J.R., Schulz, M.S., Dunham, R.E., Stern, R.J., Bloomer, S.H., 2008. Diffuse flow hydrothermal manganese mineralization along the active Mariana and southern Izu-Bonin arc system, western Pacific. J. Geophys. Res. 113, B08S14. http://dx.doi.org/10.1029/2007JB005432.
Hewett, D.F., Fleischer, M., Conklin, 1963. Deposits of the manganese oxides: supplement. Econ. Geol. 58, 1–51.
Hussein, A., 1990. Mineral deposits. In: Said, R. (Ed.), The Geology of Egypt. Taylor and Francis Publishers, London, pp. 511–566.
Iglesias, J.E., Serna, C.J., 1985. The IR spectra of hematite-type compounds with different particle shapes. Mineral. Petrogr. Acta 29, 363–370.
Jacobs, H.D., 1970. Magnetic roasting and leaching for upgrading Minnesota manganiferous iron ores: United States Bureau of Mines Bulletin, 7411 (13 pp.).
Julien, C.M., Massot, M., Poinsignon, C., 2004. Lattice vibrations of manganese oxides — part 1. Periodic structures. Spectrochim. Acta A 60, 689–700.
Klein, V., Popp, J., Tarcea, N., Schmitt, M., Kiefer, W., Hofer, S. Stuffler, Hilchenbach, T., Doyle, D., Dieckmann, M., 2004. Remote Raman spectroscopy as a prospective tool for planetary surfaces. J. Raman Spectrosc. 35, 433–440.
Krauskopf, K.B., 1957. Separation of manganese from iron in sedimentary process. Geochim. Cosmochim. Acta 12, 61–84.
Mohapatra, B.K., Mishra, P.P., Singh, P.P., Rajeev, S., 2009. Manganese ore deposits in Koira-Noamundi province of Iron Ore Group, north Orissa, India: in the light of geochemical signature. Chem. Erde 69, 377–394.
Morgan, J.J., 2005. Kinetics of reaction between O_2 and Mn(II) species in aqueous solutions. Geochim. Cosmochim. Acta 69 (1), 35–48.
Nakhla, F.M., 1961. The iron ore deposits of El-Bahariya Oasis, Egypt. Econ. Geol. 56, 1103–1111.
Nakhla, F.M., Shehata, M.R.N., 1967. Contribution to the mineralogy and geochemistry of some iron ore deposits in Egypt. Miner. Deposita 2, 357–371.
Nicholson, K., 1992. Contrasting mineralogical–geochemical signatures of manganese oxides: guides to metallogenesis. Econ. Geol. 87, 1253–1264.
Ostwald, J., 1992. Genesis and paragenesis of the tetravalent manganese oxides of the Australian continent. Econ. Geol. 87, 1237–1252.
Polgári, M., Hein, J.R., Tóth, A.L., Pál-Molnár, E., Vigh, T., Bíró, L., Fintor, K., 2012a. Microbial action formed Jurassic Mn-carbonate ore deposit in only a few hundred years (Úrkút, Hungary). Geology 40 (10), 903–906.
Polgári, M., Hein, J.R., Vigh, T., Szabó-Drubinam, M., Fórizs, I., Bíró, L., Müller, A., Tóth, A.L., 2012b. Microbial processes and the origin of the Úrkút manganese deposit, Hungary. Ore Geol. Rev. 47, 87–109.
Ramdohr, P., 1956. Die Manganerze: Symposium de1 Manganeso XX Congreso Geologico International, Mexico, Tom, 1, pp. 19–73.
Rona, P.A., 1978. Criteria for recognition of hydrothermal mineral deposits in Oceanic crust. Econ. Geol. 73, 135–160.
Roy, S., 1992. Environments and processes of manganese deposition. Econ. Geol. 87, 1213–1236.
Rull, F., Martinez-Frias, J., Rodríguez-Losada, J.A., 2007. Micro-Raman spectroscopic study of El Gasco pumice, western Spain. J. Raman Spectrosc. 38, 239–244.
Saad, N.A., Zidan, B.I., Khalil, K.I., 1994. Geochemistry and origin of the manganese deposits in the Umm Bogma region, west central Sinai, Egypt. J. Afr. Earth Sci. 19, 109–116.
Said, R., 1990. The Geology of Egypt. Elsevier, New York (734 pp.).
Salama, W., El Aref, M.M., Gaupp, R., 2012. Mineralogical and geochemical investigations of the Middle Eocene ironstones, El Bahariya Depression, Western Desert. Egypt. Gondwana Res. 22, 717–736.
Shahack-Gross, R., Bar-Yosef, O., Weiner, S., 1997. Black-coloured bones in Hayonim Cave, Israel: differentiating between burning and oxide staining. J. Archaeol. Sci. 24, 439–446.
Sung, W., Morgan, J.J., 1981. Oxidative removal of Mn(II) from solution catalyzed by the γFeOOH (lepidocrocite) surface. Geochim. Cosmochim. Acta 45, 2377–2383.
Terayama, K., Ishiguro, T., Watanabe, H., 1996. Reduction mechanism of iron–manganese oxide with carbon. Mater. Trans. 37, 1247–1250.
Tosson, S., Saad, N.A., 1974. Genetic studies of El-Bahariya iron ore deposits, Western Desert, Egypt. Neues Jb. Miner. Abh. 121, 317–393.
Urban, H., Stribrny, B., Lippolt, H.J., 1992. Iron and manganese deposits of the Urucum District, Mato Grosso do Sul, Brazil. Econ. Geol. 87, 1375–1392.
Verdonck, L., Hoste, S., Roelandt, F.F., Van der Kelen, G.P., 1982. Normal coordinate analysis of αFeOOH — a molecular approach. J. Mol. Struct. 79, 273–279.
White, W.B., Vito, C., Scheetz, B.E., 2009. The mineralogy and trace element chemistry of black manganese oxide deposits from caves. J. Cave Karst Stud. 71, 136–143.
Wilson, D.E., 1980. Surface and complexation effects on the rate of Mn(II) oxidation in natural waters. Geochim. Cosmochim. Acta 44, 1311–1317.